Transverse Initiation of an Insensitive Explosive in a Layered Slab Geometry: Front Shapes and Post-Shock Flow Measurements

Eric K. Anderson*, Tariq D. Aslam, Scott I. Jackson

Shock and Detonation Physics Group, WX-9, LANL, Los Alamos, NM 87545

Abstract

Experiments are presented that explore the shock initiating layer dynamics in an insensitive high explosive. Tests were conducted with a PBX 9502 slab bonded on one side to a PBX 9501 slab. For each test, a detonation in the PBX 9501 was generated to drive an oblique shock intended to initiate the PBX 9502. Shocks of sufficient strength generated an initiating layer, or region of delayed reaction (relative to typical PBX 9502 detonation reaction timescales) in the PBX 9502 immediately adjacent to the PBX9501. These reactions result in a transition to detonation away from the 9501/9502 interface in a process analogous to the shock-to-detonation transition in shocked one-dimensional (1D) explosive configurations. The thickness of the PBX 9501 layer was varied from 0.5 - 2.5 mm to control the strength and duration of the transmitted shock into the 8 mm thick PBX 9502. Phase velocities at the explosive outer surfaces, wave front breakout shapes, and post shock particle velocity histories associated with the detonating and initiating zones in the two explosives are reported and discussed. The initiating layer thickness decreased with increasing PBX 9501 thickness for tests with PBX 9501 thicknesses larger than 1.0 mm. A 1.0 mm thick PBX 9501 slab was not able to initiate detonation in the 8.0 mm thick PBX 9502 slab. Further decreasing the PBX 9501 thickness to 0.5 mm resulted in detonation throughout both slabs, with no initiating layer due to the intersection of each explosive's thickness effect curve at this condition. Initiating layers exhibited particle velocity profiles characteristic of non-detonating shocks. Measured phase velocities are in good agreement with DSD predictions for PBX 9501.

Keywords: detonation, shock, explosive

1. Introduction

When shocked, detonation is not immediately established in an explosive; instead, the shock travels a finite distance before transitioning to detonation. This shock-to-detonation (SDT) process allows chemical reactions in the shocked explosive to develop and couple with the shock. The SDT distance has been observed to be inversely related to the peak input shock pressure in numerous explosives. This relationship is often presented on a log-log plot, to capture the exponentially increasing sensitivity of SDT distance to shock input pressure [1]. This empirical

*Corresponding author

Email address: eanderson@lanl.gov (Eric K. Anderson)

relationship type of figure is often referred to as a "Pop-plot" after Alphonse Popolato [2]. Fig. 1 shows a Pop-plot for several explosives.

Numerous studies of initiation of TATB based explosives, including PBX 9502, have been conducted since the late 1970s, and an extensive list is provided in Gustavsen et al. [3]. These studies utilized wedge tests and gas-gun experiments to investigate the shock-to-detonation transition. Gustavsen et al. [3] conducted a series of tests where PBX 9502 instrumented with embedded gauges was impacted by gas-gun-driven projectile disks of varying thickness in order to study the effect of shock duration on SDT process. At the impact surface, the particle velocity wave form was characteristic of an inert shock. Gauges embedded further from the impact surface showed the initially inert shock wave profile transitioning to detonation-like profiles over millimeters of distance for supported shocks of sufficient duration. For very short duration impact shocks, particle velocity wave forms showed that a forward-traveling rarefaction wave caught up to the initial shock before the SDT process was complete, preventing the shock-to-detonation transition by weakening the initial shock.

If the pressure of the input shock falls below a critical value, the shock-to-detonation transition does not occur. Critical pressure is difficult to measure experimentally for the simple reason that decreasing shock pressures result in increasing run distances, and in experimental tests it is difficult to support a shock for sufficiently long durations to allow for long run distances. In a gas-gun projectile experiment, the impactor thickness would have to be increased, often beyond a practical value, to prevent the rarefaction wave from overtaking the input shock before the transition to detonation occurs. Additionally, a target of sufficiently large diameter is required to delay transverse expansion waves from reaching the shock at the center of the target.

Recovered heterogeneous explosives subjected to subcritical shock loadings have been found to be desensitized to detonation via subsequent shock compression. Such explosive has colloquially been referred to as "dead-pressed." It is thought that shock compression levels strong enough to mechanically modify the explosive but weak enough to not generate sufficient chemical reaction can desensitize the explosive via void collapse or partial reaction [4, 5]. The specific physical phenomenon responsible for this desensitization is a topic of ongoing research.

Both wedge tests and gas-gun experiments have been used to characterize shock-compressed, unreacted 1D explosive geometries. Campbell et al. [6] confined the shocked portion of RDX/TNT wedges in which the run-up to detonation occurred, and observed that detonation did not occur in this portion of the explosive. They also subjected plastic bonded HMX wedges to double shocks, showing that desensitization can occur when the first shock is at pressures too low to cause direct initiation of detonation. They attributed these observations to the prevailing theory that the explosive, when shocked at low pressure, undergoes compression and possibly subcritical reaction at voids, which increase the homogeneity of the material and reduce its sensitivity [7, 8].

To simplify the flow physics, the majority of shock-to-detonation transition and dead pressing studies have been conducted in geometries where 1D waves are generated [9]. A few past studies, however, have looked at the process in geometries where two-dimensional (2D) shock and detonation structures occur. One such configuration is that of two explosive slabs adjacent to one another. Figure 2 shows a simplified view of the detonation and shock fronts for a dual slab assembly, where the detonation velocity differs in the two explosives. On the left of the figure, the hypothetical case of the slabs detonating without any interaction is shown. The position of the detonation front in each explosive is shown at three different times ($t = 1$, $t = 2$, and $t = 3$), and it can be seen that for this case, both explosives are initiated by the booster, and the detonation in the faster explosive outruns that of the slower explosive. This behavior is not observed, however, because the faster explosive drives a shock into the slower explosive.

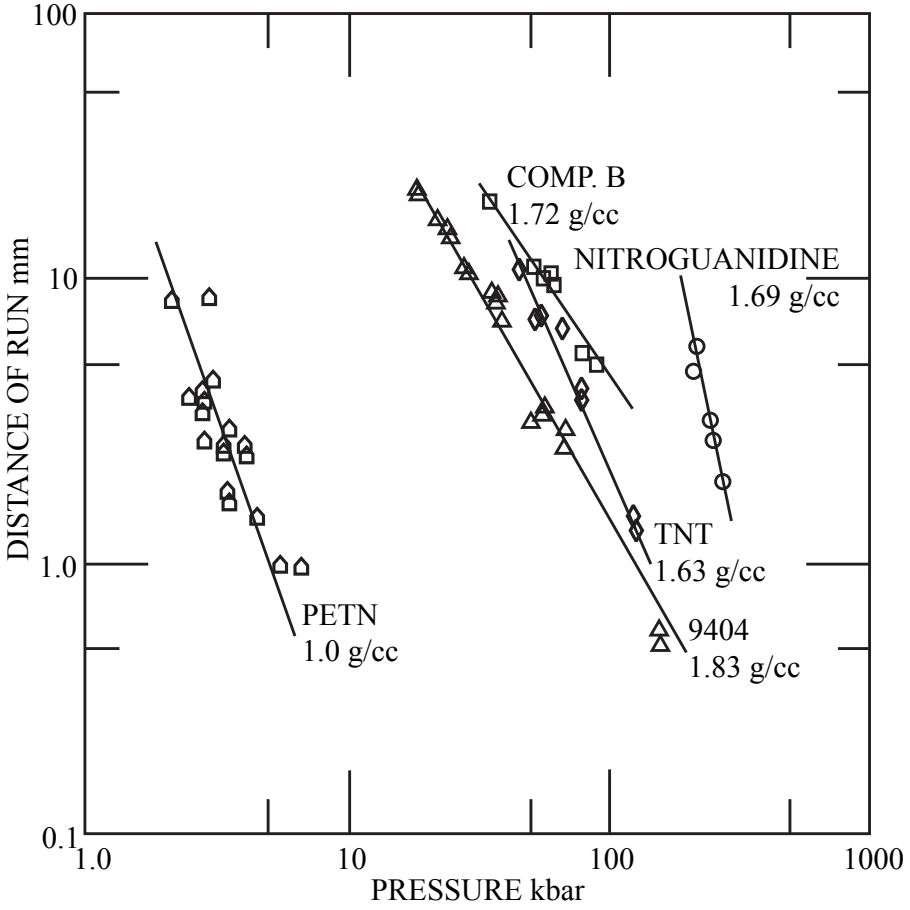

Figure 1: Pop-plot for various explosives reproduced from Ramsay and Popolato [2].

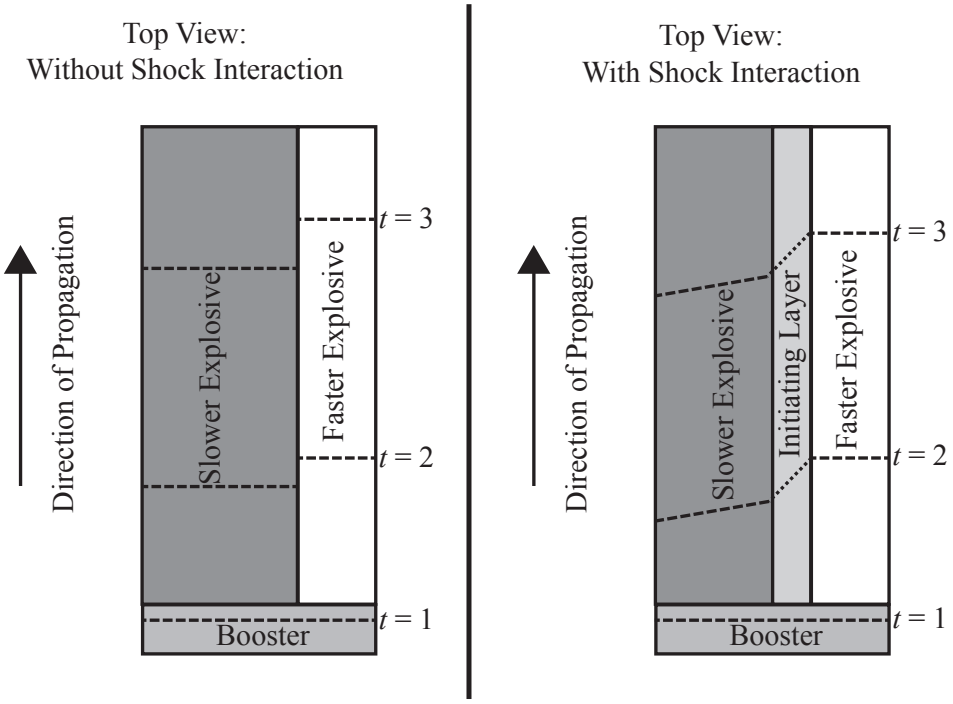

Figure 2: Expected results for a dual-slab test. The hypothetical case of the two slabs detonating without interaction is shown on the left, while the diagram on the right shows the shock and detonation structure obtained in reality, with the explosives interacting. Detonation fronts are shown with dashed lines, while inert shocks are shown with dotted lines. The regions in the explosive are colored according to the type of explosive, with the slow explosive shown darker than the fast explosive. On the right, the initiating layer, which experiences the inert shock, is shown in an intermediate color.

Often, this transmitted shock is initially not a full detonation, but rather a nearly inert shock, with normal velocities well below the Chapman-Jouguet (CJ) detonation velocity. We refer to the portion of the slower explosive experiencing the inert shock "initiating layer". Given a sufficiently strong shock from the faster explosive, a fairly abrupt transition to an oblique detonation wave occurs at the edge of the initiating layer in the slower explosive. This oblique detonation generally exhibits normal velocities near the CJ detonation velocity of the slower explosive. This detonation/inert-shock/detonation structure becomes steady a finite distance beyond the booster and then propagates at constant velocity down the explosive slabs with a steady shape.

In the late 1960s, a series of experiments with this configuration were conducted at Los Alamos. Mader [10] investigated two-layer explosive assemblies initiated by a plane wave lens placed in contact with both explosives. Flash X-ray images showed the existence of the initiating layer, immediately adjacent to the driver explosive. This region is sometimes colloquially referred to as a "dead zone" [9]. We avoid this terminology as the energy release rate and magnitude have not been measured and may not be insignificant. PBX 9404 or Composition B were used as the sensitive driver explosive, and the insensitive explosive was either X0237 (an insensitive explosive consisting of 90% TATB, 5% wax, and 5% Elvax, with a density of 1.740 g/cc) or nitroguanidine. Figure 3 shows a sample X-ray image from this series of experiments with PBX

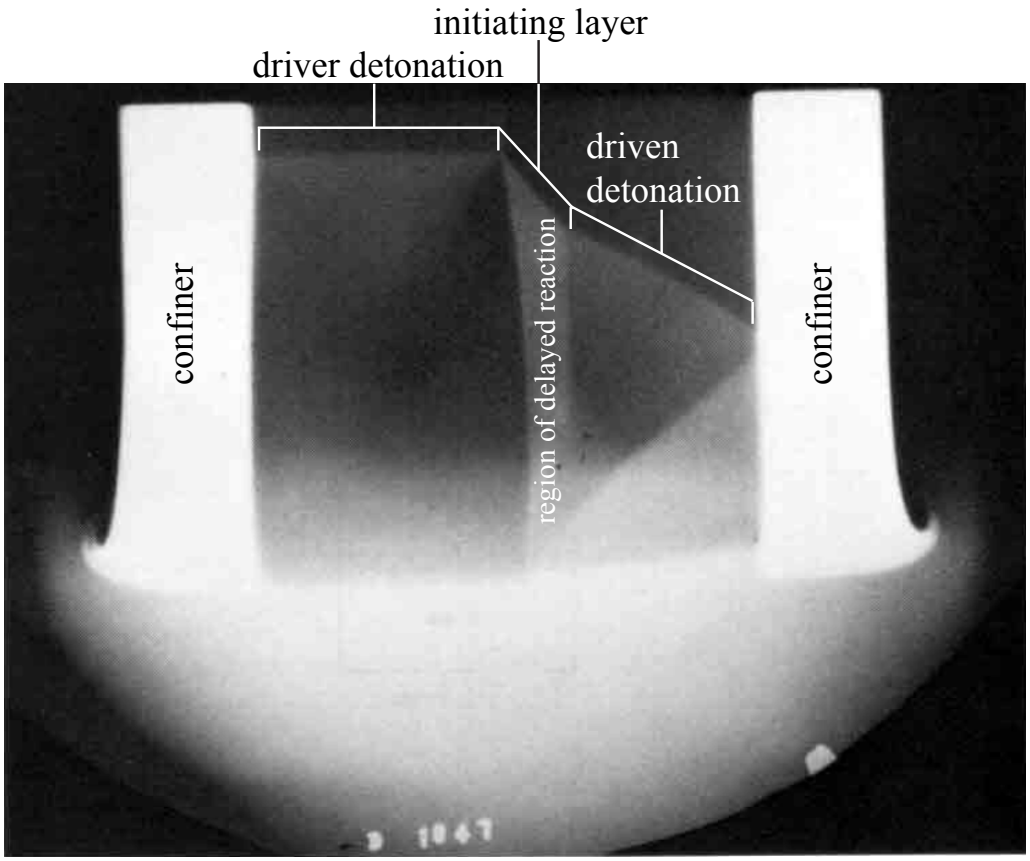

Figure 3: Flash X-ray image of PBX 9404 shocking X0237 obliquely, with the detonation traveling from the bottom to the top of the image. D. Venable, Shot 1047, LANL 1969.

9404 and X0237. In the figure, a nearly planar driver detonation is visible in the PBX 9404 on the left side of the image, and a steeply sloped, lower normal velocity initiating layer is visible in the X0237 immediately adjacent to the PBX 9404. A less steeply sloped driven detonation is visible in the remaining X0237, indicating the onset of detonation.

Matignon et al. [11] recently reported results from an experiment where an annular X1 (96% HMX, 4% binder) charge was placed in tight contact around a cylindrical T2 (97% TATB, 3% binder) charge. As in the case of the Los Alamos PBX 9404/X0237 tests, detonation in the X1 charge drove a shock and detonation structure in the T2 charge and maintained phase velocities similar to the detonation velocity in X1. An initiating layer was observed in the T2 immediately adjacent to the X1.

A similar configuration to the aforementioned PBX 9404/X0237 tests was adopted for the presently reported series of experiments, in which the behavior of PBX 9502 slabs bonded to PBX 9501 slabs along a common face is investigated. PBX 9501 is more sensitive than PBX 9502 and displays a higher detonation velocity [12]. Detonation in the faster PBX 9501 can

drive a transverse shock in the slower explosive, and in the region immediately adjacent to the faster explosive, the transverse shock is nearly inert. However, further from the interface, the transverse shock can be strengthened by developing reactions and heat release in the initiating layer and transition to full detonation.

In 1D gas-gun experiments, impactor thickness controls shock duration and impactor velocity controls the magnitude of the pressure pulse, but for the 2D layered PBX 9501/9502 explosive configurations, reducing the thickness of the PBX 9501 driving layer reduces both shock duration and pressure. Hill [13] investigated assemblies consisting of 130x150x8mm PBX 9502 bonded to 130x150x3mm thick PBX 9501, but assemblies with PBX 9501 slabs of thickness less than 3.0 mm have not been previously studied. In the present work, we vary the thickness of the PBX 9501 layer from 2.5 mm down to 0.5 mm in order to drive shocks of decreasing strength transversely into the PBX 9502 slab. By studying these assemblies, the following goals can be met:

1. Determine how the initiating layer thickness varies with driver strength (PBX 9501 thickness).
2. Identify the limiting value where the PBX 9501 will not initiate the PBX 9502.
3. Observe the initiating layer with photonic Doppler velocimetry (PDV) to record quantitative data on the reactivity of the initiating layer.

2. Experimental Assembly

The dimensions of the geometries tested are listed in table 1. The PBX 9501 thickness range was chosen to generate detonation velocities ranging from near the (CJ) velocity to much slower velocities, where the strength of the transverse shock is significantly lower, and determine the minimum thickness of the PBX 9501 layer required to initiate detonation in the PBX 9502. Table 2 lists the densities of the explosive slabs. The densities of the PBX 9502 slabs were 0.9-1.2% below the nominal value of 1.890 g/cm^3. Gustavsen et al. previously [14] showed that samples of PBX 9502 at similar densities are more sensitive, exhibiting reduced SDT distance and higher detonation velocities. Thus, the impact of below-nominal PBX 9502 density on the present work may include a small reduction in initiating layer thickness and shock angle in the detonating PBX 9502, relative to PBX 9502 at nominal density. The tested PBX 9501 slab densities were within 0.2% of the specified density of 1.836 g/cm^3.

Table 1: Measured dimensions in mm of assemblies tested. Length and width measured for PBX 9502 slab.

Length	Width	PBX 9502 Thickness	PBX 9501 Thickness
149.96	130.02	8.00	0.56
150.02	129.99	8.00	1.14
149.96	130.07	8.00	1.55
150.00	130.00	8.00	2.00
150.01	130.02	8	2.5

Table 2: Measured densities of assemblies tested.

PBX9501 Thickness (mm)	PBX 9501 Density (g/cm^3)	PBX 9502 Density (g/cm^3)
0.5	1.8354	1.8719
1.0	1.8346	1.8697
1.5	1.8355	1.8722
2.0	1.8327	1.8704
2.5	1.8342	1.8675

Figure 4 shows an image of the explosive assembly with the 2.0-mm-thick PBX 9501 layer, and Fig. 5 shows the assembly geometry, which is an adaption of that described in Hill and Aslam [15]. The initiating shock train consisted of a RP-2 detonator (mfg. by Teledyne RISI Inc.), line wave detonation generator, and an 8 mm x 8 mm x 150 mm Composition B booster bonded to one 150 mm edge of the slab assembly. The booster was aligned with the outer PBX 9501 face of the assembly, and hence not in full contact with the PBX 9502 layer, due to the fact that the 9501/9502 assemblies were thicker than 8 mm. Full contact with the PBX 9502 was not critical due to the fact that detonation in the PBX 9501 drives the PBX 9502 detonation faster than initiation and detonation of the PBX 9502 by the booster. As described in [15], the length and width of the assembly was chosen to produce a 2D, steady wave structure near the center of the assembly (where streak camera and PDV measurements are taken). This is due to the fact that the length of the assembly is chosen such that release waves moving in from the line wave generator edges do not influence the measurements at these locations.

For each assembly, the PBX 9501 was bonded to the PBX 9502 using Angstrom Bond AB9320. To achieve good contact between the explosive layers, the assembly was placed in an aligning fixture under approximately 6 bar pressure as the epoxy cured. Eleven evenly spaced ionization wires were taped to each exposed 150 x 130 mm face, starting 30 mm from the booster. These wires are visible in the side view of Fig. 5 for the PBX 9502 face. Also visible in the break-out face view are the streak camera imaging surface and three PDV probes indicated by small circles. One probe was located 0.5 mm from the PBX 9501/9502 interface on the PBX 9502. The other two were centered on the PBX 9501 and on the PBX 9502. For the shots with the 2.5, 1.5, and 1.0-mm-thick PBX 9501, each PDV probe was bonded to two stacked LiF windows, each of 9.4 mm diameter and 5 mm thickness. For the shots with the 2.0 and 0.5-mm-thick PBX 9501, each probe was bonded to a single LiF window of 12.7 mm diameter and 12.7 mm thickness.

3. Results and Analysis

3.1. Framing Camera

For each test, a Cordin 550 framing camera was focused on the PBX 9502 slab (same view as the side view of Fig. 5) to provide high-speed video. The camera was operated at 800,000 frames per second with 250 ns integration times. Figure 6 shows framing camera images at 7.5 μs intervals for the assemblies with 1.0, 1.5, 2.0, and 2.5 mm thick PBX 9501 layers. The times

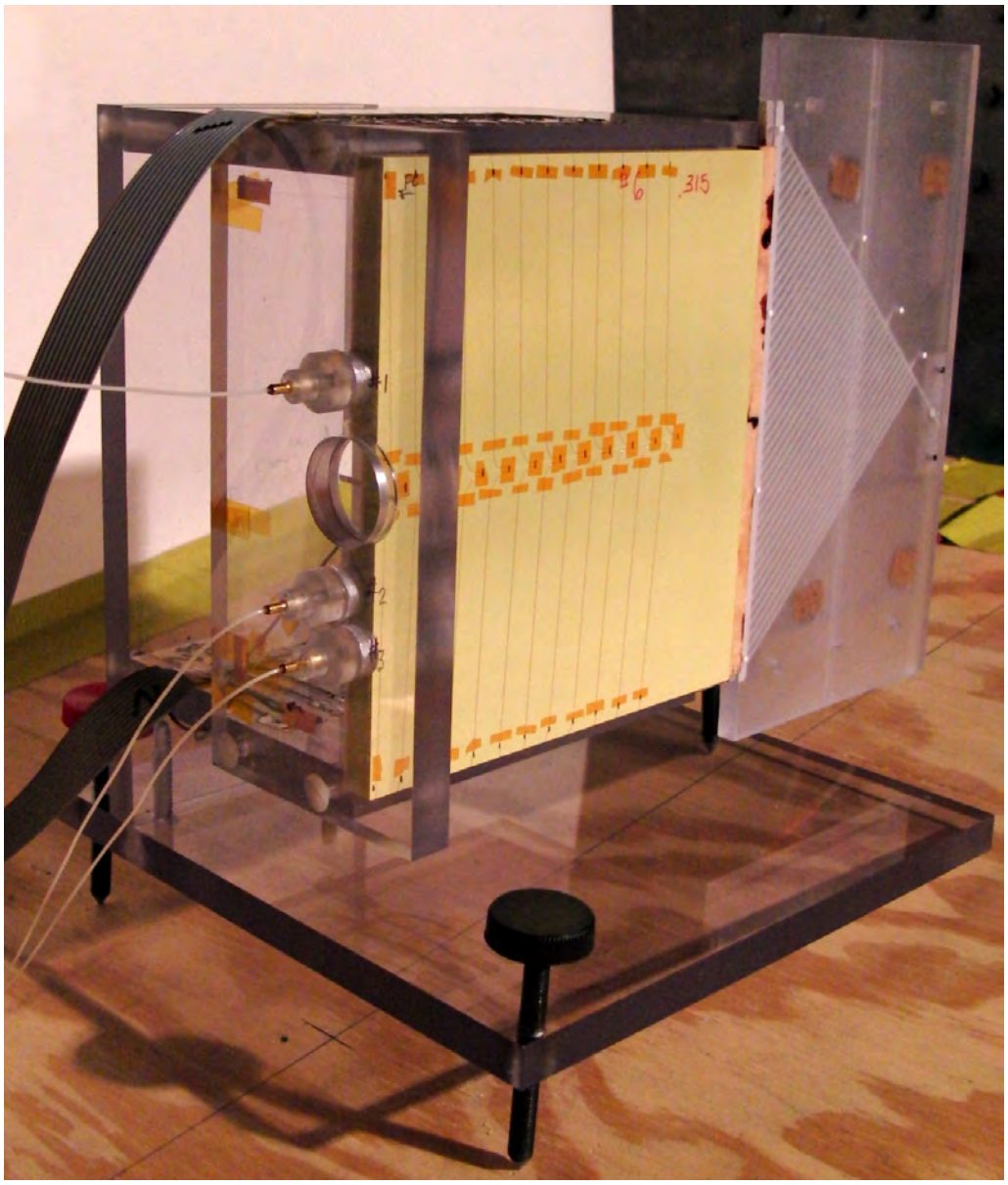

Figure 4: Perspective view showing the PBX 9502 side of explosive assembly.

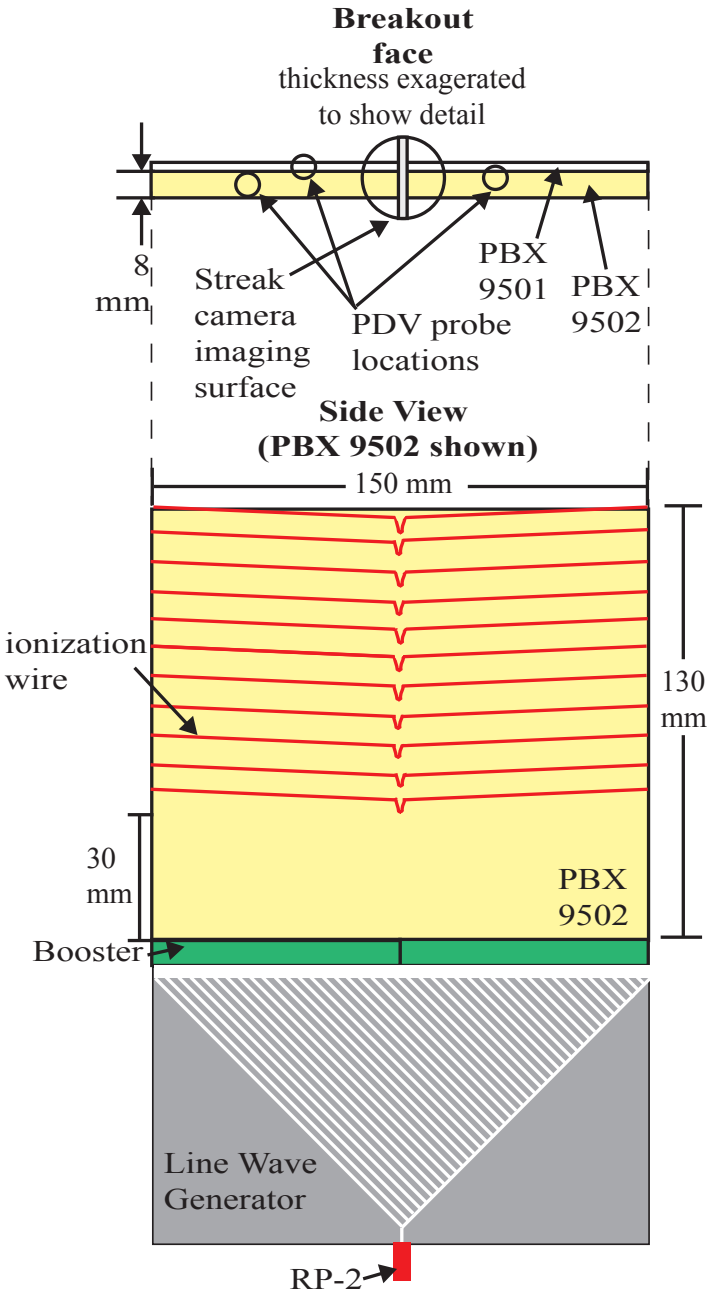

Figure 5: Diagram of explosive assembly showing key dimensions.

specified in the figure indicate time after detonator trigger. The CCD-specific gain varied from 22-400 for each test.

Differences in camera magnification between the shots exist due to variations in shot placement, but several important differences between the four shots displayed are apparent. At 22.5 μs after detonator trigger, it can be seen that the detonation front travels slightly faster on the PBX 9502 side as PBX 9501 thickness is increased, due to the thickness-effect phenomenon in the PBX 9501.

At 30 μs after detonator trigger, the PBX 9502 detonation has reached the end of the explosive assembly with the 2.5, 2.0, and 1.5-mm-thick PBX 9501 layers. For the assembly with the 1.0-mm-thick PBX 9501 layer, the detonation appears to have only consumed 75% of the PBX 9502, and intense light is visible at the end of the explosive assembly despite the fact that there is still undetonated PBX 9502 visible. This is due to the fact that the detonation has reached the end of the PBX 9501 slab. Subsequent frames from the Cordin 550 camera show detonation appearing to fail in the PBX 9502 slab in the 1.0 mm case before the entire slab is consumed.

3.2. Ionization Wires

Ionization wires 0.05 mm in diameter were placed on both sides of the explosive assemblies approximately every 9 mm starting after a 30-mm run distance from the Comp B booster. The positions of the ionization wires were recorded to within ± 0.5 μm using a binocular microscope equipped with a 3-axis translation stage. The resulting spatial data were combined with temporal data recorded on an oscilloscope sampling at 5 GS/s with 1 GHz bandwidth. For each side of the explosive assemblies, a linear fit to the ionization wire time-position data was computed, and the slope was extracted as the phase velocity. Sample ionization wire position-time data are shown in Fig. 7.

Table 3 displays the ionization wire results from all five assemblies. For the assemblies with 1.5, 2.0, and 2.5-mm-thick PBX 9501 layers, linear fits were obtained with standard errors less than 0.006 mm/μs, which is below 0.1% of the reported velocities. The low standard errors indicate that, for these shots, steady detonation waves were observed. The phase velocities on the PBX 9501 side decreased slightly with decreasing PBX 9501 layer thickness. For these assemblies, the phase velocity measured on the PBX 9502 side was approximately 0.1% slower than on the PBX 9501 side.

For the assembly with the 0.5-mm-thick PBX 9501 layer, the phase velocities were substantially lower, at 7.496 mm/μs on the PBX 9501 side and approximately 0.4% lower on the PBX 9502 side. The decrease in velocities for this test were expected due to the thickness effect in the PBX 9501 slab. The standard error was quite low for the PBX 9502 side, indicating a steady wave, but higher on the PBX 9501 side, indicating a slightly less steady wave.

The results for the assembly with the 1.0-mm-thick PBX 9501 layer are particularly interesting. The phase velocity on the PBX 9501 side of the assembly was steady and relatively fast at 8.441 mm/μs. However, on the PBX 9502 side, the phase velocity was nearly 1.0 mm/μs slower than the PBX 9501 side and approximately 0.1 mm/μs slower at the breakout end of the shot than at the first ionization wire. From the phase velocities, it appears that at this PBX 9501 thickness, the shock driven in the PBX 9502 was insufficient to sustain PBX 9502 detonation. The variation in PBX 9502 phase velocity from one end of the shot to the other indicates a decrease in wave velocity at the end of the explosive. Framing camera data in Fig. 6 shows that for this shot, a detonation was initiated and consumed slightly more than 50% of the PBX 9502 slab, but failed in the last 40 mm of the explosive as the shock from the adjacent PBX 9501 pushed the PBX 9502 away with insufficient strength to support detonation.

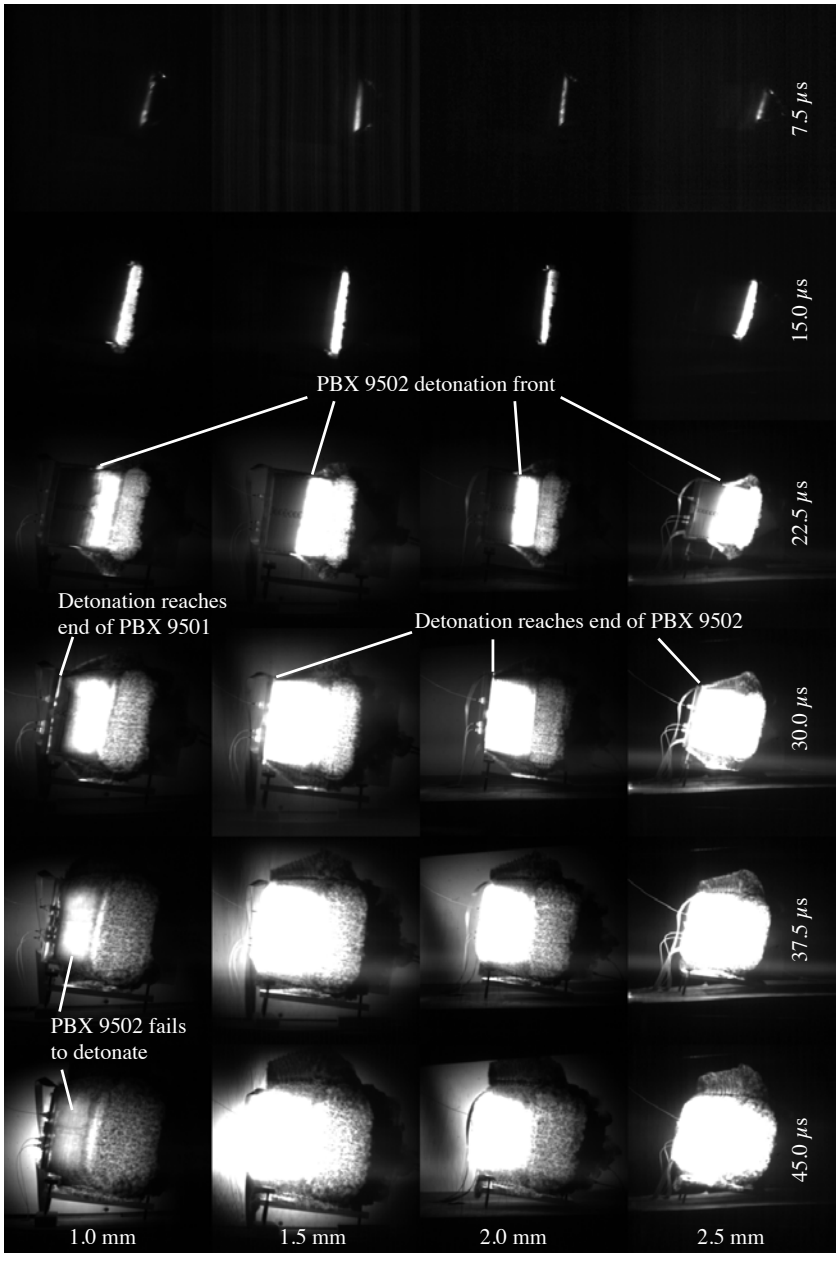

Figure 6: Framing camera images with each column representing a different test with the PBX 9501 thickness indicated at the bottom. Each row represents a different time after detonator trigger, indicated on the right. Important features are labeled in the figure.

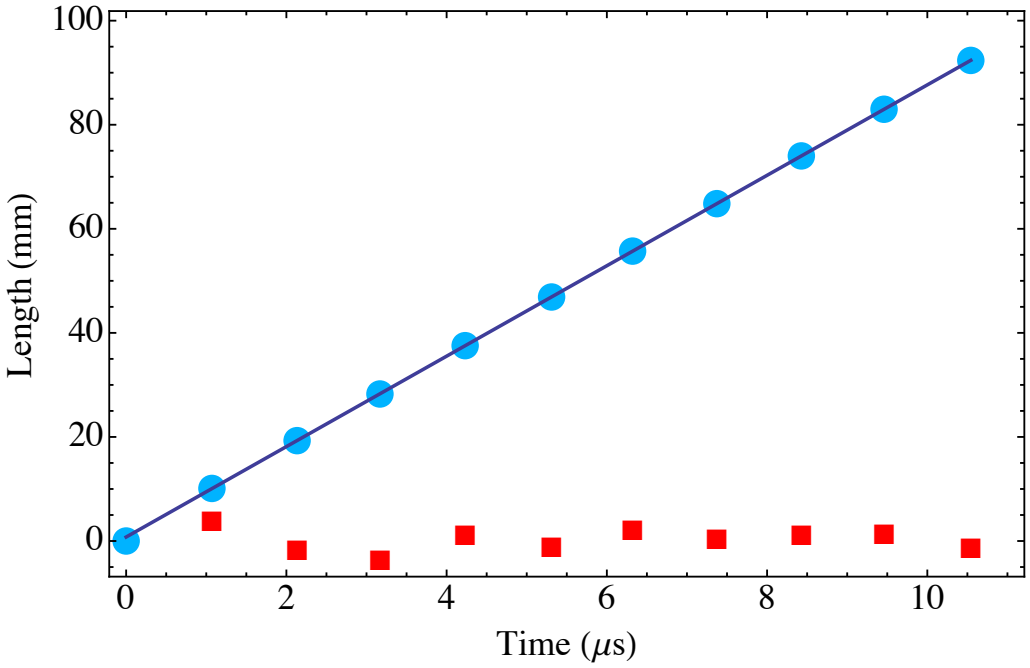

Figure 7: Ionization wire phase velocity data from the assembly with the 2.0-mm-thick PBX 9501 layer. Raw data are represented by ●, the line represents the linear fit, and ■ indicate fit residuals ×100.

Table 3: Phase velocities measured with ionization wires.

PBX 9501 Thickness (mm)	PBX 9501 Phase Velocity (mm/μs)	PBX 9501 Standard Error (mm/μs)	PBX 9502 Phase Velocity (mm/μs)	PBX 9502 Standard Error (mm/μs)
0.5	7.496	0.041	7.470	0.002
1.0	8.441	0.002	7.50-7.62	0.130
1.5	8.638	0.002	8.623	0.005
2.0	8.696	0.001	8.690	0.002
2.5	8.731	0.001	8.723	0.006

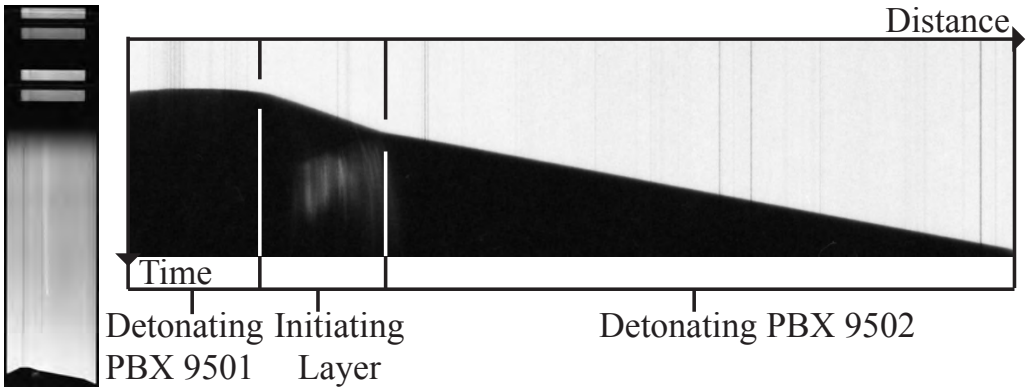

Figure 8: Streak camera film scan (left) and result of rotation and cropping (right) for 1.5-mm-thick PBX 9501 layer assembly. Approximate boundaries of the breakout regions are shown.

3.3. Streak Camera Image Processing

For each shot, two still images were recorded with a streak camera prior to detonation and recording the streak image, as shown in Fig. 8. The still images were used to determine the horizontal-scaling and the edges of the explosive slabs on the streak image. The streak image cropped to include only the breakout in the explosive slabs is shown on the right in Fig. 8.

Approximately 1000 points/mm along the shock breakout were then manually selected with an uncertainty of ± 1 pixel for both the detonating and the initiating regions in the PBX 9502 (as labeled in Fig. 8). The manually selected set of coordinates with units of pixels then required conversion to physical length units in both the vertical and horizontal directions.

The vertical direction of the streak camera film represents time, not distance, and was converted to a time-scale using the image write speed associated with the Cordin 132 streak camera. Next, the phase velocity measured with the ionization wires was used to convert from time to distance in the vertical direction on the film. The result yielded the shape of the wave at breakout from the explosive. For sufficiently flat wave shapes, the breakout process is supersonic and transverse flow associated with the initial shock breakout does not influence the wave shape

in neighboring regions. Assuming a bulk sound speed of 3.28 mm/μs and a bulk velocity of 7.4 mm/μs, shock angles less than approximately 66 ° in PBX 9502 satisfy this condition. For higher bulk velocities, the threshold angle is even higher. All of the tests reported here satisfy the condition with the exception of slower portions of the test with the 1.0-mm-thick PBX 9501 slab, where the normal velocity dropped below 4.5 mm/μs. Cropped front curvature images for all five explosive assemblies are shown in Fig. 9, where all five shots are scaled uniformly. The magnification in the horizontal direction is double that of the vertical direction, as indicated at the lower left of the figure.

Beginning with the case of the 0.5-mm-thick PBX 9501 assembly, a gently curved shock front is visible, with greater curvature at the exposed PBX 9502 face. Some jetting is visible at the PBX 9501/9502 interface, which is likely detonation product jetting ahead of the detonation, indicating a possible air gap between the glued explosive slabs. The 1.0-mm-thick PBX 9501 assembly generated a divergent detonation in the PBX 9501 with a steeply sloped front in the PBX 9502. It can be seen that the shock in the PBX 9502 was slightly concave toward the shocked explosive, with a steeper slope away from the PBX 9501, indicating higher normal velocities near the PBX 9501 due to support by the adjacent detonation. The 2.5, 2.0, and 1.5-mm-thick PBX 9501 assemblies displayed similar shock front morphology, with a divergent shock front in the PBX 9501, a steeply sloped, slightly divergent front (characteristic of the initiating layer) in the roughly 1.0 mm of immediately adjacent PBX 9502, and a less steeply sloped near-linear front in the rest of the PBX 9502. It can be seen that the thickness of the initiating layer decreased with increasing PBX 9501 thickness, consistent with the understanding that stronger shocks have a shorter shock-to-detonation transition distance.

The manually selected points along the shock fronts were used to compute linear fits in the detonating and initiating regions. Figure 10 displays the front curvature for the assembly with the 1.5-mm-thick PBX 9501 layer. The slope from the linear fit was used to determine the shock angle,

$$\phi = \arctan(b) \tag{1}$$

where ϕ is the shock angle and b is the slope of the shock. Having computed ϕ, the normal shock velocity is

$$D_n = D_0 \cos(\phi) \tag{2}$$

where D_n is the normal shock velocity and D_0 is the phase velocity. The above equations were used to determine shock angle and normal shock velocity for both detonating and initiation regions. Figure 10 shows the definition of these variables graphically.

For each of the five assemblies, linear fits were computed for each point along the shock front using the neighboring points. The window size for computation of these linear fits was varied from 0.16 mm to 0.8 mm in steps of 0.16 mm. Results of this fitting process are shown in Figs. 11 - 15, along with the front shape from the streak camera (the front shape is plotted against the right ordinate axis for each figure, where the vertical scaling is determined using the image write speed of the camera, but the magnitude is arbitrary). For the case of the 0.5-mm-thick PBX 9501 assembly, shown in Fig. 11, the shock front is divergent, and it can be seen that normal velocities of around 7.5 mm/μs are found from 0 to 6 mm into the explosive. Normal velocities do not vary greatly as a function of linear fit window size for this case. Near the exposed face of the PBX 9502, normal velocities decrease sharply due to edge expansion effects at the free surface. These edge effects were present for all five shots, and for the cases of the 2.5 - 1.5-mm-thick PBX 9501 assemblies, data within 0.25 mm of the edge was not used to compute the linear fit for the reported normal velocity. For final computation of normal velocity (shown by the dashed

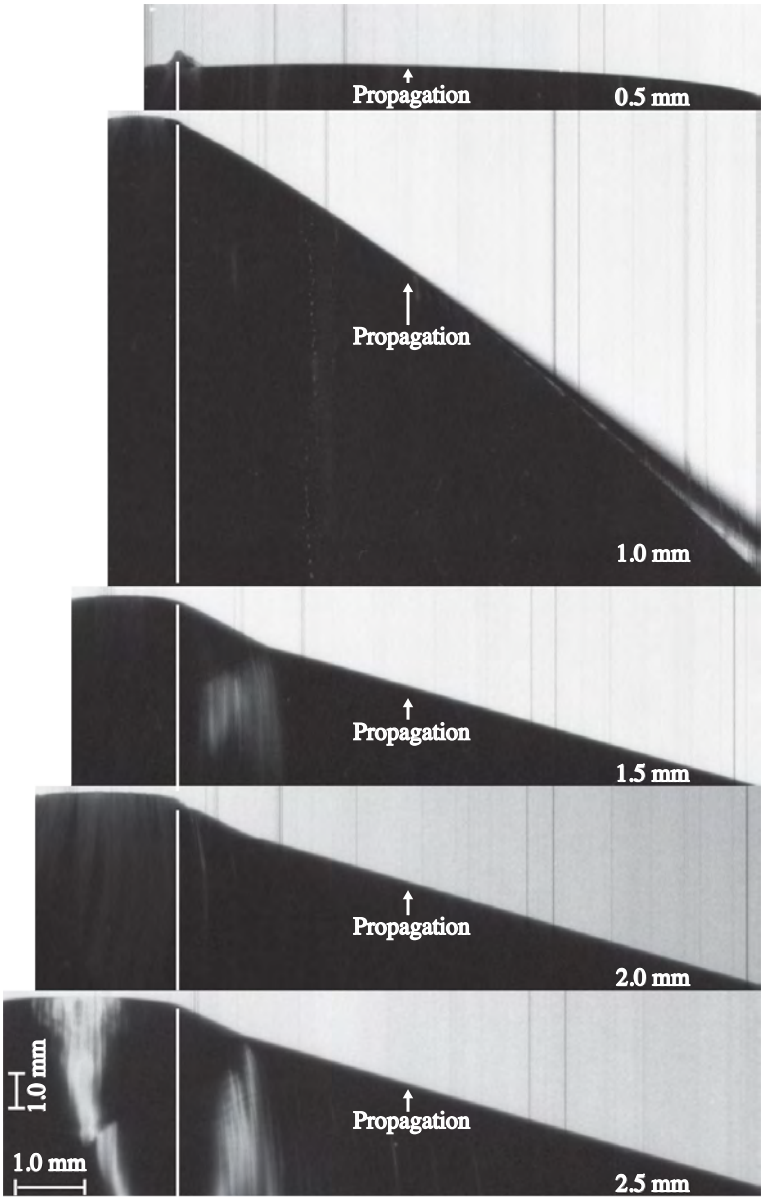

Figure 9: Cropped and scaled streak camera film scans for all five assemblies. Approximate boundary between PBX 9501 and PBX 9502 indicated by the white lines, with PBX 9502 on the right. For each image the thickness of the PBX 9501 layer is indicated on the lower right.

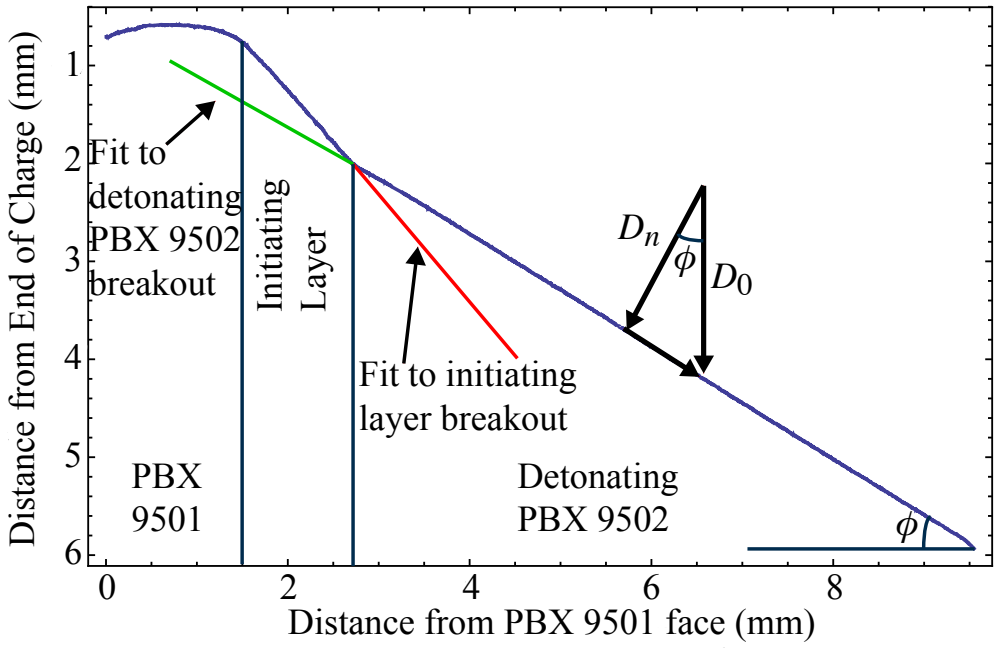

Figure 10: Front shapes for the 1.5-mm-thick PBX 9501 layer assembly. Shock angle and shock normal velocity are labeled on the left, and the intersection used to determine initiating layer thickness is shown on the right.

black lines of Figs. 13 - 15), the linear fit region was manually chosen to discard data influenced by edge effects based on visual inspection of the linear fits computed with the 0.16 - 0.80 mm windows.

Figure 12 displays results from the 1.0-mm-thick PBX 9501 assembly. Here, slight curvature in the shock front is visible near the PBX 9501 interface, and normal velocity decreases from over 5.0 mm/μs to below 4.5 mm/μs as distance from the interface increases. These velocities are below 65% of the PBX 9502 Chapman-Jouguet velocity and indicate that this wave is not a detonation. For this case, noise in the normal velocity curve increases as linear fit window size decreases, due to increased fitting error associated with smaller window sizes.

Figures 13 - 15 display results from the 2.5 - 1.5-mm-thick PBX 9501 assemblies. These three shock fronts have similar morphology with a clearly visible initiating layer and detonating layer. For each of these figures, initiating layer is visible on the left, with non-linearity apparent in the initiating layer front shape as changing slope and hence normal velocity. Normal velocities in the initiating layer vary from 5.8 to 6.5 mm/μs. The window sizes of 0.16 to 0.8 mm are on the order of the $\approx$ 1 mm initiating layer thickness. For this reason the fits displayed in Figs. 13 - 15 are not able to capture initiating layer velocity accurately. Instead, the initiating layer normal velocities reported in table Table 4 are the result of a single linear fit to the points between the PBX 9501/9502 interface and the shock to detonating transition point.

The transition from initiating layer to detonating PBX 9502 is seen in Figs. 13 - 15 as a large increase in normal velocity over a short distance. The criterion used herein to determine the demarcation point between the initiating layer and detonating PBX 9502 was the maximum slope location of the normal velocity curves. This transition point is displayed on the figures as a vertical line colored corresponding to each window size. Due to the short distance over which the shock transitions from initiating layer to detonating PBX 9502, the smallest window (0.16 mm) for the linear fits was used for determination of the transition point.

For all three cases in Figs. 13 - 15, except for noise of magnitude inversely related to linear fit window size, the normal velocity was nearly constant over a region indicated on the figures by black-horizontal-dashed lines. These lines indicate the region over which the detonating normal velocity was computed, and their position represents the computed value. These three shots all display a drop in normal velocity near the unconfined face of the PBX 9502, as expected due to transverse flow expansion across the free surface. Interestingly, they also display an overshoot in normal velocity between the transition point and the constant normal velocity, detonating PBX 9502, possibly due to overdrive associated with the shock-to-detonation transition process.

Initiating layer thickness and normal velocity data computed using a single linear fit over the initiating layer are shown for each explosive assembly in Table 4. Small standard errors are associated with the fits with the exception of the fit to the initiating layer of the 1.0 mm thick PBX 9501 assembly. In this case a linear profile does not adequately describe the physics, but is used to concisely summarize the behavior. The second column shows the normal velocity for the detonating region in the PBX 9502, and for the assemblies with PBX 9501 layers of 2.5-1.5 mm thickness, were approximately 7.5 mm/μs. For these cases the initiating layer normal velocities were over 1.0 mm/μs slower, and the initiating layers were approximately 1.0-mm thick and decreased with increasing PBX 9501 layer thickness. The assembly with the 0.5-mm-thick PBX 9501 layer displayed no initiating layer. Instead, both explosive layers were initiated by the Composition B booster and both detonated at approximately the same speed due to thickness effects in both explosives yielding similar detonation velocities in this assembly. The PBX 9502 detonation front showed slight curvature, resulting in a normal velocity varying from 7.0-7.5 mm/μs depending on the distance from the PBX 9501 slab. For the case of the 1.0-mm-thick

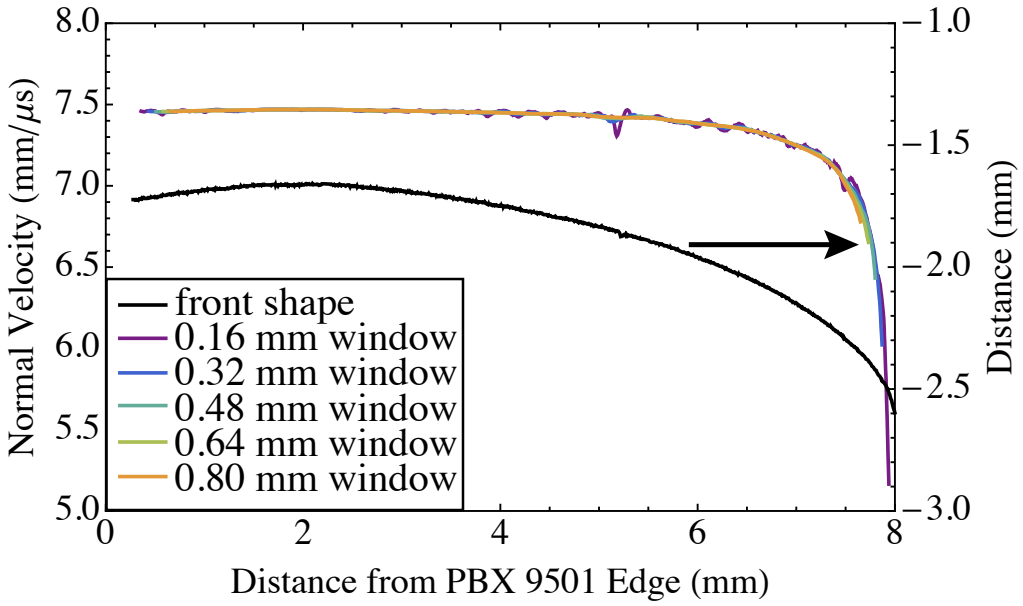

Figure 11: Normal velocity (colors) and front shape (black, right ordinate axis) in PBX 9502 as a function of distance from PBX 9501 interface (on left) for the 0.5-mm-thick PBX 9501 assembly.

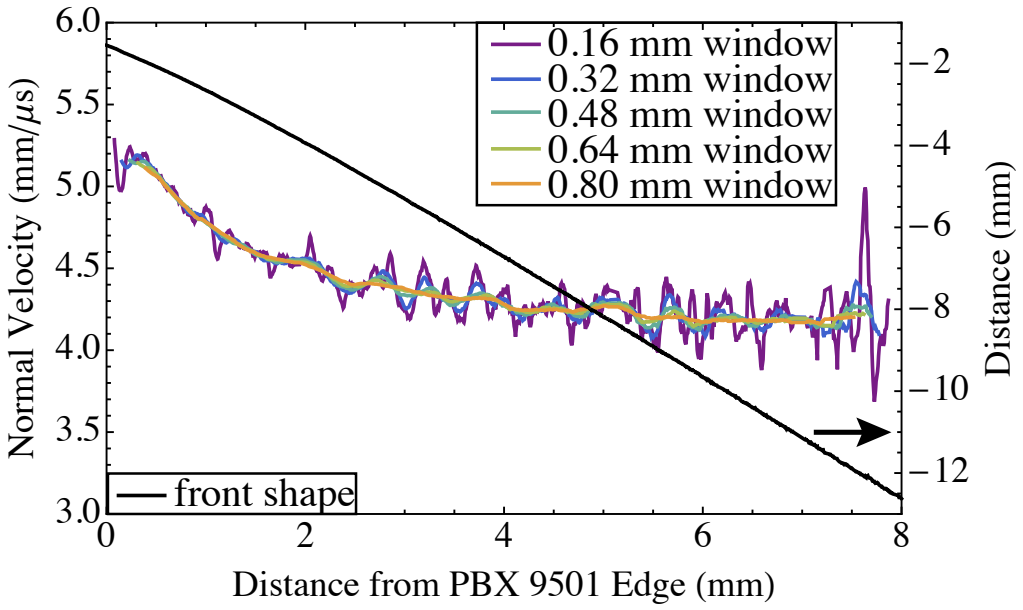

Figure 12: Normal velocity (colors) and front shape (black, right ordinate axis) in PBX 9502 as a function of distance from PBX 9501 interface (on left) for the 1.0-mm-thick PBX 9501 assembly.

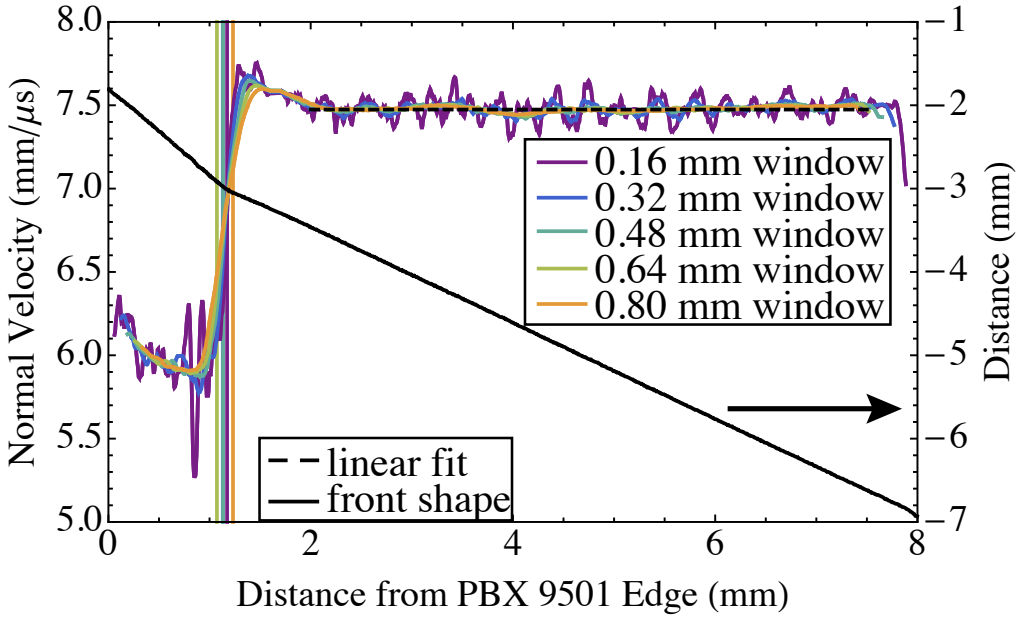

Figure 13: Normal velocity (colors) and front shape (black, right ordinate axis) in PBX 9502 as a function of distance from PBX 9501 interface (on left) for the 1.5-mm-thick PBX 9501 assembly. Linear fit used to extract normal velocity and vertical lines indicating transition from initiating layer to detonation also shown (black, dashed).

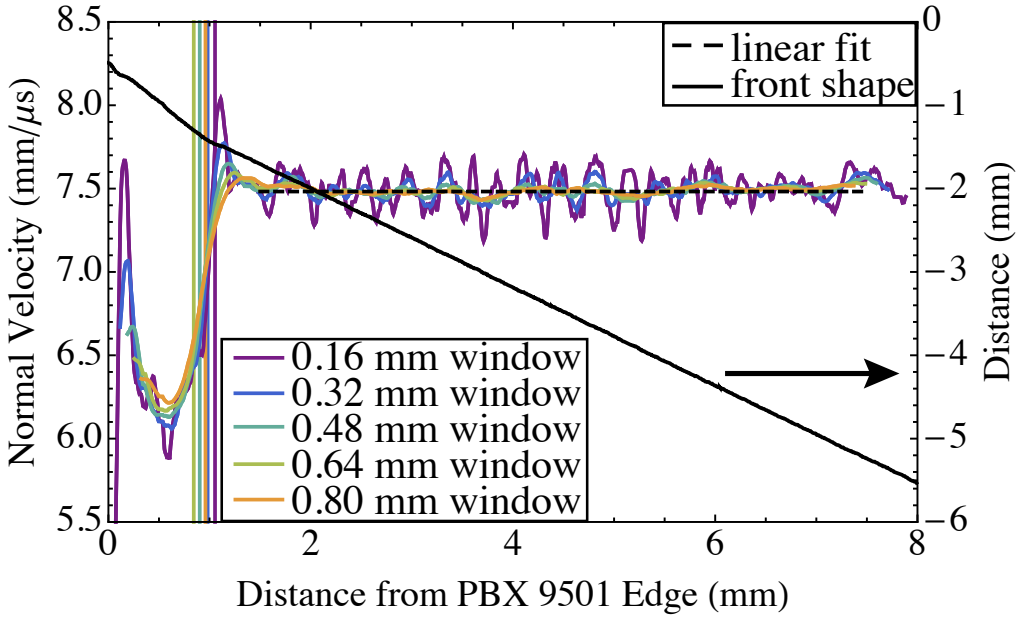

Figure 14: Normal velocity (colors) and front shape (black, right ordinate axis) in PBX 9502 as a function of distance from PBX 9501 interface (on left) for the 2.0-mm-thick PBX 9501 assembly. Linear fit used to extract normal velocity and vertical lines indicating transition from initiating layer to detonation also shown (black, dashed).

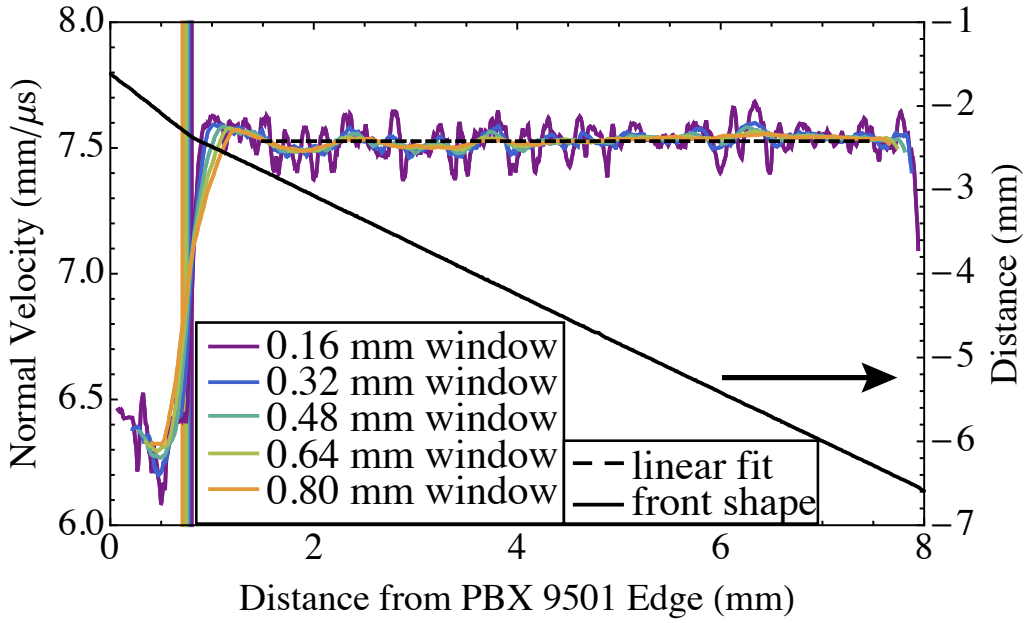

Figure 15: Normal velocity (colors) and front shape (black, right ordinate axis) in PBX 9502 as a function of distance from PBX 9501 interface (on left) for 2.5-mm-thick PBX 9501 assembly. Linear fit used to extract normal velocity and vertical lines indicating transition from initiating layer to detonation also shown (black, dashed).

PBX 9501 assembly, the entire PBX 9502 slab behaved as the initiating layer. At approximately 4.1 mm/μs, the lowest PBX 9502 normal velocities were observed in this test, and a steady wave profile was not established within the 130 mm length of the explosive assembly.

Table 4: Streak camera results for 1.5, 2.0, and 2.5 mm PBX 9501 assemblies. A range of PBX 9502 normal velocities was observed for the assembly with the 0.5 mm PBX 9501 slab due to shock front curvature.

PBX 9501 Thick-ness mm	PBX 9502 Normal Velocity mm/μs	Std. Error mm/μs	Initiating Layer Normal Velocity mm/μs	Std. Error mm/μs	Initiating Layer Thick-ness mm
0.5	7.15-7.47	0.002	none	none	none
1.0	none	none	4.11-5.06	0.080	>8
1.5	7.474	0.004	5.950	0.004	1.17
2.0	7.482	0.002	6.373	0.005	1.05
2.5	7.526	0.005	6.310	0.005	0.80

The initiating layers described in Table 4 are shown graphically in Fig. 16 for tests with PBX 9501 slabs of 1.0 to 2.5 mm thickness. Since initiating layer was not observed for the test with the 0.5 mm PBX 9501 layer, it is excluded from this figure. For the results from assemblies with 2.5 to 1.5 mm PBX 9501 layers, the transition to from initiating layer to detonation is clearly visible as a change in slope of the shock front shape. In addition to increasing thickness of the initiating layer, the slope of the igniting layer increases with decreasing PBX 9501 thickness. For the assembly with the 1.0 mm PBX 9501 layer, the trend of increasing slope with decreasing PBX 9501 thickness continues, though the transition to detonation did not occur.

3.4. Photonic Doppler Velocimetry

PDV is a laser-based heterodyne interferometry technique used to measure the velocity of a reflective target. It is based on the fact that the beam reflected off a moving target undergoes a Doppler shift, and when this light is combined with a fraction of the original beam, an interference pattern is generated. The beat frequency of this interference pattern is proportional to the velocity of the target in the direction of the reflected beam [16].

For each shot in the series reported here, PDV probes were placed as indicated by the small circles on the breakout face in Fig. 5. One probe was located on the PBX 9502 slab 0.5 mm from the interface with the PBX 9501 slab, while the other two were centered on the PBX 9501 and PBX 9502 slabs. All probes used in this test series had a 100 μm spot size. Each probe was placed on one side of a LiF window, and the other side of the window was coated with vapor-deposited aluminum. The aluminum-coated side of the window was placed against the explosive. The dimensions of the LiF windows used in each shot are provided in Section 2. In this configuration, the probes provide particle velocity data of the explosive product-LiF window interface. All three probes were located far enough away from the top and bottom of the assembly to avoid significant three-dimensional curvature effects near the edges.

The output of the PDV system was recorded on a 20 GHz oscilloscope sampling at 50 GS/s. This data was analyzed by computing the fast Fourier transform and relating the frequency of

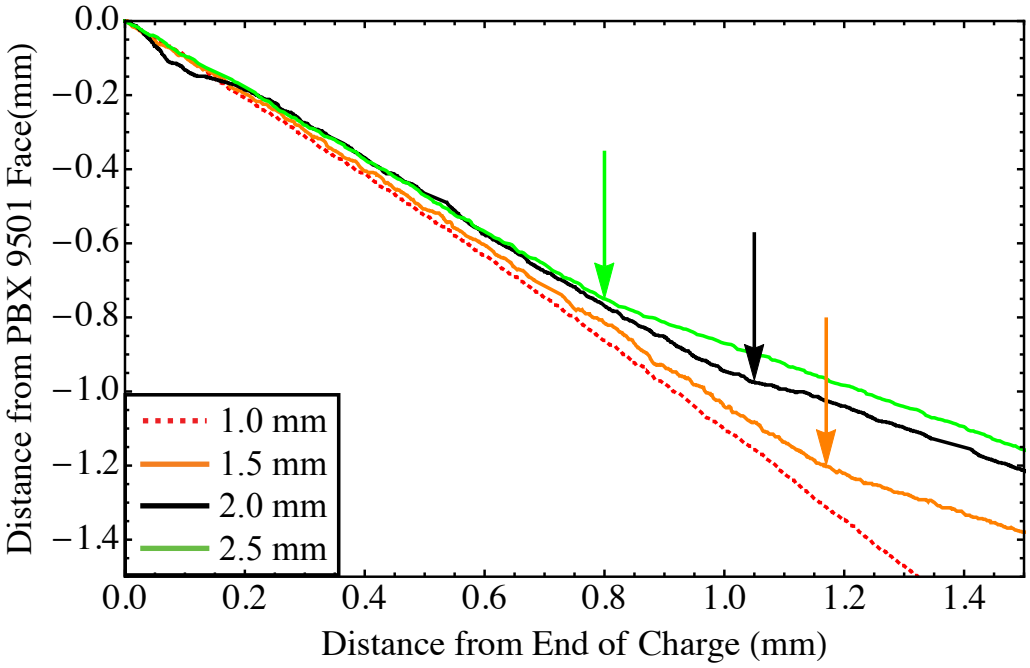

Figure 16: Streak camera front shapes zoomed in on the region around the initiating layer for tests with PBX 9501 layer thicknesses indicated in the legend. Arrows indicate the location of the initiating layer to detonation transition as reported in Table 4.

the signal to particle velocity. The Fourier transform was computed using a window size of 1024 samples and window step of 128 samples. The velocities computed were reduced by a factor of 1.2669 to account for the index of refraction of the LiF windows [17].

Figures 17-19 show the processed PDV results for all three probe locations and all five explosive assemblies. The results from Fig. 17 show that all five assemblies displayed PDV profiles characteristic of detonating explosive at the probe location centered on the PBX 9501, with an almost discontinuous acceleration to high velocity followed by a gradual relaxation to approximately 0.5 mm/μs due to flow expansion.

The PDV velocity profiles measured by the probe centered on the PBX 9502, displayed in Fig. 18, were characteristic of detonating explosive for the 0.5, 1.5, 2.0, and 2.5-mm-thick PBX 9501 assemblies, but not the 1.0-mm-thick PBX 9501 assembly. For the 0.5-mm-thick PBX 9501 assembly, the velocities recorded during the first 0.5 μs after shock-up were greater than the other three detonating cases. The streak camera record from this test showed that the PBX 9502 detonation was not driven by the PBX 9501, but rather detonated independently of the PBX 9501. This resulted in higher post-shock pressure and normal velocity, and the less steeply sloped detonation produced particle velocities more closely aligned with the PDV measurement axis. The PDV probe centered on the PBX 9502 generated a velocity profile characteristic of a non-detonating shock for the 1.0-mm-thick PBX 9501 assembly. This result is consistent with the streak camera record which shows initiating layer throughout the entire thickness of the PBX 9502 slab for this shot. PDV measurements, however, allow for increased observation time, and this probe indicated little-to-no reaction during the 1.4 μs observation window.

Results from the probes located on the PBX 9502 0.5 mm from the PBX 9501 interface are displayed in Fig. 19. This location was chosen to place the probe over the expected location of the initiating layer. The initiating layer is characterized by a shock traveling below 90% of the Chapman-Jouguet detonation velocity, without reaction behind the shock during the measurement time of the PDV diagnostic ($\approx$ 1.4 μs). All PDV measurements of the initiating layers produced velocity profiles characteristic of inert shocks, displaying a slow rise to a peak velocity substantially lower than that of detonation waves. From the figure, it can be seen that this probe location captured the initiating layer for the assemblies with the 1.0, 1.5, 2.0, and 2.5-mm-thick PBX 9501 slabs. The PDV profiles for these assemblies are reminiscent of what is observed in embedded gauges in the 1D shock-to-detonation buildup experiments of Gustavsen et al. [3]. Clearly this is only a qualitative comparison as these waves are oblique and are measurements at the PBX 9502/LiF window interface, while embedded gauges measure particle velocities within the explosive. However, these results can be used with LiF and PBX 9502 Hugoniot data in reactive model simulation. Finally, in the case of the 0.5-mm-thick PBX 9501 assembly, a PDV profile characteristic of detonation was observed, confirming the streak camera results showing detonation across the entire thickness of the assembly. This is the first published PDV measurement of initiating layer in an explosive assembly exhibiting 2D wave structure and quantifying (in velocity-time space) the low level of reaction present relative to detonating flows. These data will be useful to researchers developing flow models that resolve detonation reaction zones and shock-pressure-dependent initiation phenomenon.

4. Comparison to Modeling Predictions

For the range of PBX 9501 layer thickness tested, the Detonation Shock Dynamics (DSD) model [18] has been calibrated to predict the phase velocity of PBX 9501 detonating unconfined without adjacent explosive [19]. DSD predicts detonation propagation velocities by relating the

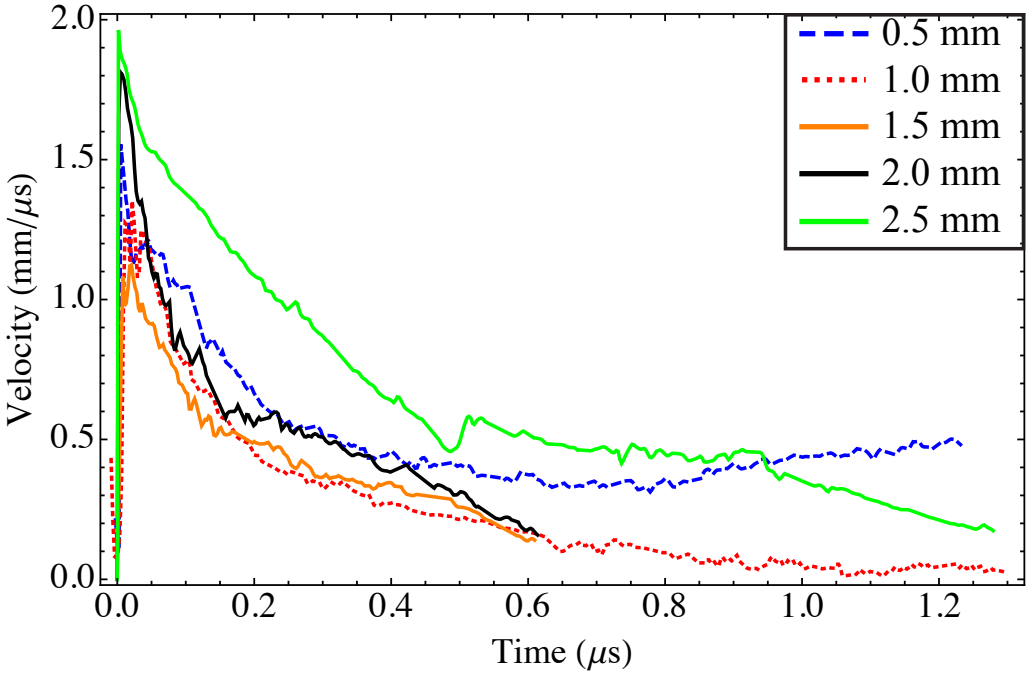

Figure 17: PDV velocity profiles from the probe centered on the PBX 9501 slab for five explosive assemblies. Legend indicates PBX 9501 thickness.

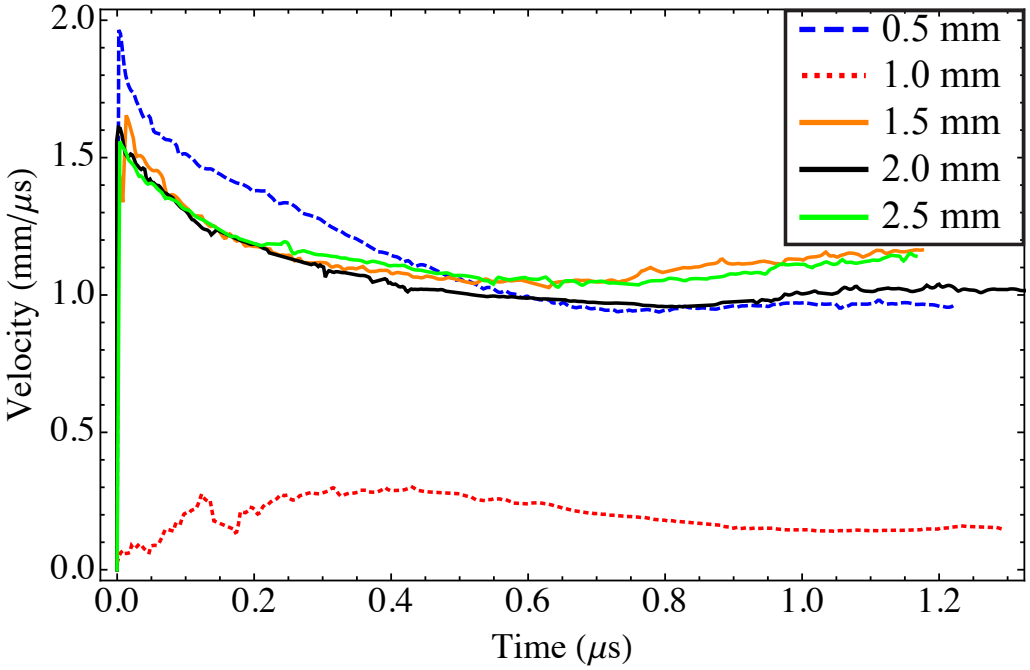

Figure 18: PDV velocity profiles from the probe centered on the PBX 9502 slab for five explosive assemblies. Legend indicates PBX 9501 thickness.

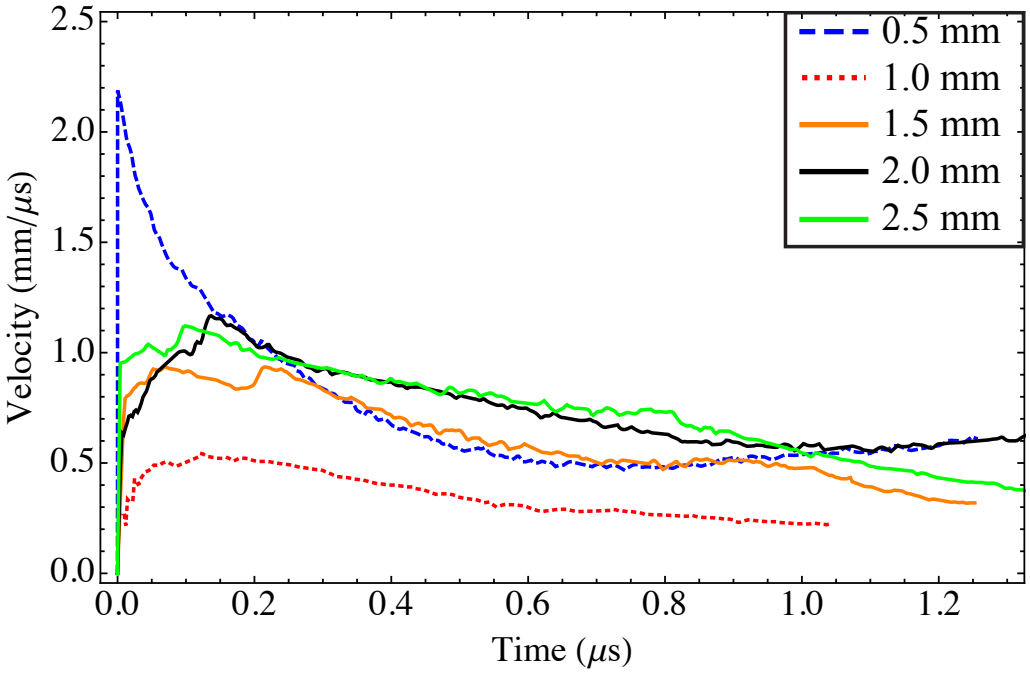

Figure 19: PDV velocity profiles from the probe located on the PBX 9502 slab 0.5 mm from the PBX 9501/9502 interface (initiating layer location). Legend indicates PBX 9501 thickness.

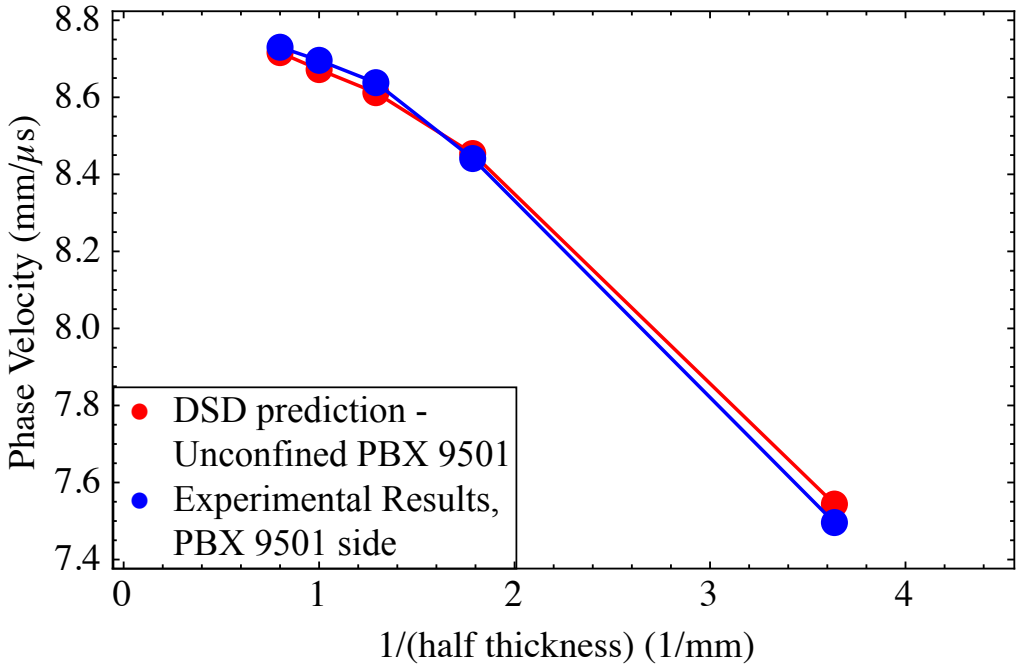

Figure 20: PBX 9501 thickness effect curves, as computed by DSD and measured from the PBX 9501/9502 explosive assemblies.

normal speed of the detonation wave, D_n, to the local curvature, κ. For a given explosive, the DSD model must be calibrated using experimental D_n vs. κ data. The calibrated DSD model may then be used to predict the time evolution of a detonation wave in new geometries. DSD results, along with the experimental results measured for the PBX 9501/9502 assemblies are shown in Fig. 20, with the DSD fit parameters used to generate this figure provided in Appendix A.

The DSD results under-predict experimental phase velocity results by 0.1 - 0.3% for PBX 9501 layers thicker than 1.0 mm, and over predict the phase velocity for the 0.5 and 1.0-mm-thick PBX 9501 layers by 0.6%. The DSD results generally agree well with the experiments, with the largest discrepancy 0.6% of the predicted value. DSD under-prediction of phase velocities could be due to the edge angle choice at the PBX 9501/9502 interface (edge angles were chosen for a slab unconfined on both sides).

5. Summary and Conclusions

Explosive assemblies consisting of an 8.0-mm-thick PBX 9502 slab bonded to a PBX 9501 slab ranging from 0.5 to 2.5-mm-thick were tested experimentally. Each assembly was instrumented with ionization wires to measure phase velocities, and detonation breakout was imaged with a streak camera. In addition, PDV probes were placed on the breakout end of the assembly to measure explosive-LiF window interface velocities in each explosive and the initiating layer. By decreasing the thickness of the PBX 9501 layer, the strength of the shock driven into the PBX 9502 slab was also decreased. This had the effect of increasing the initiating layer thickness, or

shock-to-detonation distance in the transverse direction. The detonation velocity in the PBX 9501 layer was also affected by its thickness, and for the smallest assembly tested, the detonation velocity in the PBX 9501 slab matched that of the PBX 9502 slab.

The experimental results from shorting wires are summarized in table 3, and results from the streak camera are summarized in table 4. Based on these measurements, as well as the PDV results of Figs. 17-19, the results fall into three distinct steady wave configurations based on the thickness of the driving HE:

1. *Fast HE initiates slow HE*. Here, similar phase velocities are observed for both PBX 9501 and PBX 9502, with the phase velocity being dictated by the PBX 9501. For this configuration, both an initiating layer and a detonating layer were observed in the PBX 9502. The normal velocity in the detonating PBX 9502 appears to be close to the 1D CJ detonation velocity. Initiating-layer PDV probes (located on the PBX 9502, 0.5 mm from the interface between the two explosives) recorded velocity profiles characteristic of inert shocks. This flow regime was displayed by the assemblies with PBX 9501 layers of 1.5, 2.0, and 2.5-mm-thickness. This flow regime was also observed for prior 3.0 mm thick PBX 9501 experiments as well [13].
2. *Fast HE fails to initiate slow HE*. The case of the 1.0 mm PBX 9501 layer demonstrates a boundary between the two steady wave configurations of 1 and 3. For this case, a steady shock front was observed in the PBX 9501, but not in the PBX 9502 within the 130 mm length of the explosive. Both the initiating layer PDV probe and the centered PBX 9502 probe recorded velocity profiles characteristic of inert shocks. One would need a PBX 9502 slab thicker than 8mm to transit to detonation, if it would transition to detonation at all.
3. *Coupled fast and slow HE detonation*. This flow regime was displayed by the assembly with the 0.5 mm PBX 9501 slab. For this assembly, the PBX 9501 and PBX 9502 were both initiated by the Composition B booster and detonated at nearly equal velocities. This assembly and likely even thinner slabs of PBX 9501 represent the case where the PBX 9501 cannot naturally detonate faster than the PBX 9502, thus the detonation structure is likely a function of the composite HE assembly.

These results will assist in the validation of reactive flow models intended to accurately predict shock-to-detonation processes in multi-dimensional geometries. Future work will quantify the post-shock pressures associated with the observed initiating layers relative to 1D Pop-plot data. Such a comparison is expected to provide insight into the influence of 2D flow geometry on the SDT initiation process.

Acknowledgments

This effort was funded by the U.S. Department of Energy Campaign 2: “Dynamic Material Properties.” Experiments were assembled and fielded with assistance provided by Sam Vincent and Tim Tucker.

Appendix A.

The $D_n(\kappa)$ formulation used to compute the results of Fig. 20 is

$$\frac{D_n}{D_{CJ}} = 1 - B\kappa\left(\frac{1 + c_2\,(B\kappa)^{e_2} + c_3\,(B\kappa)^{e_3}}{1 + c_4\,(B\kappa)^{e_4} + c_5\,(B\kappa)^{e_5}}\right), \tag{3}$$

where $e_2 = e_4 = 1$ and $e_3 = e_5 = 2$ [19], D_n is the local shock normal velocity, and κ the local shock curvature. The fitting parameters are given in Table 5. The value of D_{CJ} used in equation 3 was computed as a function of density using the equations $D_{CJ} = D_{CJ_{nominal}}(1 + c_6(\rho_0/\rho_{0_{nominal}} - 1))$ and $c_6 = \rho_0 \times 4.135/D_{CJ_{nominal}}$, where ρ_0 is the measured density of the unreacted PBX 9501 slab. The value of B was computed using the equation $B = B_{PBX9501}(\rho_0/\rho_{0_{nominal}})^{c_7}$. The value of κ_{max} is assumed for all $\kappa \geq \kappa_{max}$, and was increased to 5 mm^{-1} to extrapolate to the thinnest PBX 9501 sample. It should be noted that extrapolation had to be used because this sample is outside the range of DSD calibration data in Aslam and Short [19]. The parameter ω_s is the complement to the shock deflection angle, and the value was chosen assuming both faces of the PBX 9501 slab were exposed to atmospheric air.

Table 5: PBX 9501 DSD parameters [19].

$D_{CJ_{nominal}}$	8.811 mm/μs
$\rho_{0_{nominal}}$	1.836 g/cm^3
κ_{max}	5 mm^{-1}
$B_{PBX9501}$	1.66374 mm
c_2	17.5036
c_3	3.15931
c_4	554.576
c_5	0.185264
c_6	0.861634
c_7	1.26499
ω_s	0.9408

References

[1] P. W. Cooper, Explosives Engineering, Wiley-VCH, New York, NY, 1996.
[2] J. B. Ramsay, A. Popolato, in: 4th Symposium (Int.) on Detonation, Office of Naval Research, 1965, pp. 233–237.
[3] R. L. Gustavsen, S. A. Sheffield, R. Alcon, J. Appl. Phys. 99 (2006).
[4] S. A. Sheffield, R. Engelke, R. R. Alcon, in: Ninth Symposium (Int.) on Detonation, Office of Naval Research, 1989, pp. 39–49.
[5] J. Zhang, T. Jackson, J. Buckmaster, J. Freund, Combust. Flame 159 (2012) 1769–1778.
[6] A. W. Campbell, W. C. Davis, J. B. Ramsay, J. R. Travis, Phys. Fluids 4 (1961) 511–521.
[7] E. F. Gittings, in: Fourth Symposium (Int.) on Detonation, Office of Naval Research, 1965, pp. 373–380.
[8] A. W. Campbell, J. Travis, in: Eighth Symposium (Int.) on Detonation, Office of Naval Research, 1985, pp. 1057–1068.
[9] W. C. Davis, The Dead Zone, Technical Report LA-UR-08-05456, Los Alamos National Laboratory, 2008.
[10] C. L. Mader (Ed.), LASL Phermex Data Volume III, Los Alamos Series on Dynamic Material Properties, University of California Press, Berkeley, CA, 1980.
[11] C. Matignon, R. Sorin, O. Bozier, in: Fourteenth Symposium (Int.) on Detonation, Office of Naval Research, 2010, pp. 1182–1190.
[12] T. R. Gibbs, A. Popolato (Eds.), LASL Explosive Property Data, Los Alamos Series on Dynamic Material Properties, University of California Press, Berkeley, CA, 1980.

[13] L. Hill, in: Shock Compression of Condensed Matter, American Institute of Physics, 2013.
[14] R. L. Gustavsen, D. G. Thompson, B. W. Olinger, R. Deluca, B. D. Bartram, T. H. Pierce, N. J. Sanchez, in: Fourteenth Symposium (Int.) on Detonation, Office of Naval Research, 2010, pp. 655–663.
[15] L. G. Hill, T. D. Aslam, American Institute of Physics, 2003, pp. 847–850.
[16] P. D. Sargis, N. E. Molau, D. Sweider, M. E. Lowry, O. T. Strand, Photonic Doppler Velocimetry, Technical Report URCL-ID-133075, Lawrence Livermore National Laboratory, 1999.
[17] B. J. Jensen, D. B. Holtkamp, P. A. Rigg, J. Appl. Phys. 101 (2007).
[18] J. B. Bdzil, D. S. Stewart, Shock Wave Sci. Technol. Ref. Libr. 6 (2012) 373–453.
[19] T. Aslam, M. Short, Detonation Shock Dynamics Overview and Calibration, Technical Report LA-UR-13-26358, Los Alamos National Laboratory, 2013.